14

Two and Three Dimensional Extreme Ultraviolet Holographic Imaging with a Nanometer Spatial Resolution

P. W. Wachulak[1] and M. C. Marconi[2]
[1]*Military University of Technology, Institute of Optoelectronics*
[2]*NSF ERC for Extreme Ultraviolet Science & Technology and Department of Electrical and Computer Engineering, Colorado State University*
[1]*Poland*
[2]*USA*

1. Introduction

The word "hologram" (from the greek *"holos"*: whole, complete and *"graphos"*: writing, drawing) means "total recording". Holography is a well known technique originally proposed in 1948 by Gabor, who also coined the name, as a new microscopy alternative. He realized that the interference of two mutually coherent waves, one called the reference wave and the second one - the object wave, allows for recording of information consisting of both amplitude and phase of diffracted or scattered beam from an object (Gabor, 1948). This coding of the amplitude and phase of the object beam into an interference pattern allowed him to demonstrate that from this complicated holographic pattern, ultimately the image of the original object can be obtained. Several years after the appearance of Gabor's paper, Baez (Baez, 1952) suggested extension of this idea to the X-ray region, but it remained as an interesting proposal till the early 1960s, when holography started to be widely applied. It was after the paper by Leith and Upatnieks, who proposed the off-axis holography - scheme which overcomes many of Gabor configuration drawbacks (Leith & Upatnieks, 1962). Since that time holography was widely used in numerous applications, some of them requiring increased spatial resolution. On this path, reducing the illumination wavelength is a direct way to improve spatial resolution both in nanopatterning (Solak et al., 1999; Wachulak et al., 2008a) and holographic imaging, described herein. This is the reason why short wavelength sources such as synchrotrons, extreme ultraviolet (EUV) and soft X-ray (SXR) lasers, high harmonics generation sources (HHG), etc., became an interesting alternative for high resolution imaging.

This chapter is devoted to 2-D and 3-D holographic imaging using a capillary discharge EUV laser. The chapter is organized as follows. In section 2 recent developments in high resolution holographic imaging will be briefly presented including different imaging techniques and short wavelength sources. In section 3 some general information about Gabor in-line EUV holography will be presented with detailed analysis of the resolution limitations due to coherence of the EUV source and digitization process. Starting from section 4 through 6 recent developments in holographic 2-D and 3-D imaging will be

presented (Wachulak et al., 2010). In section 4 a 2-D holographic imaging using a compact EUV laser, the experimental details, results and resolution estimation using a wavelet decomposition and correlation method will be discussed. The resolution of the 2-D holographic imaging was further improved by increasing the recording/reconstruction numerical aperture, leading to spatial resolution comparable to the illumination wavelength, approximately 46nm (section 5). A novel method of resolution and feature size assessment, based on a Gaussian filtering and correlation was applied and the results were compared with well established, knife-edge resolution test. Finally in section 6 a 3-D holographic recording and reconstruction, that allowed for successful 3-D information retrieval from a single high numerical aperture EUV hologram, will be presented. Section 7 concludes the chapter.

2. Developments in high resolution EUV and soft X-ray holographic imaging

The potential for holography in the EUV region was recognized very early. However realization of this goal become very difficult, thus only in the early 1970s the first images of very simple objects were obtained for the first time (Giles, 1969; Aoki & Kikuta, 1974). The main obstacle to record and reconstruct good quality holograms in this region of e-m spectrum was lack of sufficiently bright and coherent sources. It was not until 1987 that the high resolution x–ray imaging was realized by use of 2.5–3.2 nm SXR radiation from the National Synchrotron Light Source (NSLS), where spatial resolution of 40 nm was demonstrated. Fourier transform holography at the NSLS achieved spatial resolution of 60 nm (McNulty et al., 1992). Gabor holography with an early X-ray laser pumped by two beams of the fusion-class NOVA laser at Lawrence Livermore National Laboratory demonstrated a spatial resolution of 5 μm (Trebes et al., 1987).

Other experiments utilized synchrotron light to image biological samples, nano structures, and magnetic domains (Jacobsen et al., 1990; Lindas et al., 1996; McNulty et al., 1992). Lens-less diffractive imaging, based on iterative phase retrieval, following the proposal by Sayre, (Sayre et al., 1998) have demonstrated SXR imaging with 50 nm spatial resolution utilizing λ = 1.5 nm source (Elsebitt et al., 2004). The first experimental demonstration of lens-less diffractive imaging using coherent soft X-rays generated by a tabletop SXR source allowed for image acquisition with spatial resolution of 214 nm (Sandberg et al., 2007) later improved to 72 nm (Sandberg et al., 2008). High resolution scanning X-ray diffraction microscopy proved to be a useful imaging technique employing coherent, short wavelength radiation, reaching spatial resolution better than 70 nm (Thibault et al., 2008).

The practical demonstration of EUV and SXR holography proved to be difficult in particular because the lack of sufficiently bright and coherent sources at short wavelengths, and to the fact that coherent EUV and SXR laser sources have historically been restricted to large user facilities. The first demonstration of a coherent table-top holographic imaging achieved 7 μm spatial resolution with a spatially-coherent HHG source (Bartels et al., 2002); this resolution has been extended to a resolution of 0.8 μm in later experiments (Morlens et al., 2006). Time resolved holographic imaging was also implemented with HHG sources to study the ultrafast dynamics of surface deformation with a longitudinal resolution of less than 100 nm and a lateral resolution of less than 80 μm (Tobey et al., 2007). Holography was also used to demonstrate 100 nm-resolution holographic aerial image monitoring based on lens-less Fourier transform holography at EUV wavelengths, using synchrotron-based illumination (Hun Lee et al., 2001). Femtosecond EUV radiation provided by the free-electron laser

FLASH was used for digital in-line holographic microscopy to image particles, diatoms and critical point dried fibroblast cells with 620 nm spatial resolution at 8 nm wavelength (Rosenhahn et al., 2009). Digital in-line SXR holography (DIXH) was used to image immobilized polystyrene and iron oxide particles with spatial resolution of 850 nm at wavelength range of 3.7-5.6 nm to take advantage of selective contrast in this wavelength range (Rosenhahn et al., 2008). Holographic measurement scheme to monitor the X-ray-induced explosion of microscopic objects was performed by a femtosecond time-delay X-ray holography, inspired by Newton's "dusty mirror" experiment, allowed to see the changes in EUV induced explosion of 140 nm diameter polystyrene beads (Chapman et al., 2007). By combining HHG holography with iterative phase retrieval algorithm, usually employed in diffractive lens-less imaging, reconstructed hologram spatial resolution was improved to ~53 nm (Sandberg et al., 2009). Holograms can be also obtained in very short exposure times. Using uniformly redundant arrays (URA) instead of a single or multiple reference pinholes in Fourier type holography the throughput of the imaging system might be sufficiently large to acquire a hologram with a single 15 fs EUV pulse and reconstruct with spatial resolution approaching 50 nm (Marchesini et al., 2008). Naturally, the body of knowledge related to this topic is so immense, that we are not able to mention all the work done in the field, only some aspects of it.

3. Gabor in-line EUV holography

The acquisition of holographic images is a two step process consisting of recording and reconstruction phase. The holographic recording in Gabor's in-line configuration is depicted in Fig. 1a. During the recording step the interference pattern between two mutually, collinear and coherent beams is stored in the recording medium. The two interfering beams are the reference beam (black dashed lines) and the object beam (green solid lines). The recording medium is a material used to record the interference pattern that can provide a linear mapping between the incident intensity and some kind of change in the medium such as the reflection, transmission or height modulation. If the object and reference wavefronts are both expressed as a two complex fields having amplitudes and phases:

$$o(x,y) = \left|o(x,y)\right| e^{j\phi(x,y)} \tag{1}$$

$$r(x,y) = \left|r(x,y)\right| e^{j\psi(x,y)} \tag{2}$$

then the interference between these two complex fields occurring at the location of the recording medium can be expressed as the intensity distribution of sum of two fields:

$$\begin{aligned} I(x,y) &= \left|r(x,y) + o(x,y)\right|^2 = \left[r(x,y) + o(x,y)\right]\left[r(x,y) + o(x,y)\right]^* = \\ &= \left|r(x,y)\right|^2 + \left|o(x,y)\right|^2 + r^*(x,y)\cdot o(x,y) + o^*(x,y)\cdot r(x,y) \end{aligned} \tag{3}$$

The first two terms are the intensities of both interfering beams, while the last terms depend also on their phases. That is why the recording medium, sensitive only to the intensity, is in fact capable of storing the intensity and the phase information simultaneously.
The linear mapping of the recording medium can be described as transmission change of the recording medium (for example photographic film) as a function of the incident intensity:

$$t(x,y) = t_0 + \kappa \cdot I(x,y) \tag{4}$$

where t_0 is the uniform transmittance of the film introduced by the constant exposure and κ is a linear factor relating the transmission to the incident intensity $I(x,y)$. By substituting equation Equation (3) into Equation (4) the transmission of the recording medium can be thus expressed as:

$$t(x,y) = t_0 + \kappa \cdot \left[|r(x,y)|^2 + |o(x,y)|^2 + r^*(x,y) \cdot o(x,y) + o^*(x,y) \cdot r(x,y) \right] \tag{5}$$

This interference pattern, stored in the recording medium during the reconstruction step, acts as a complicated diffraction grating. If the intensity of the interference pattern during the recording step is linearly translated into a recording medium transmission then the reconstruction step is similar to the one depicted in Fig. 1b. The hologram is placed in the same geometry and illuminated by the same wavefront as in the recording step, now called reconstruction wavefront. This can be expressed as:

$$\begin{aligned} u(x,y) = r(x,y) \cdot t(x,y) = r(x,y)\left(t_0 + \kappa \cdot |r(x,y)|^2 \right) + \kappa \cdot r(x,y) \cdot |o(x,y)|^2 + \\ \kappa \cdot o(x,y) \cdot |r(x,y)|^2 + \kappa \cdot o^*(x,y) \cdot |r(x,y)|^2 \end{aligned} \tag{6}$$

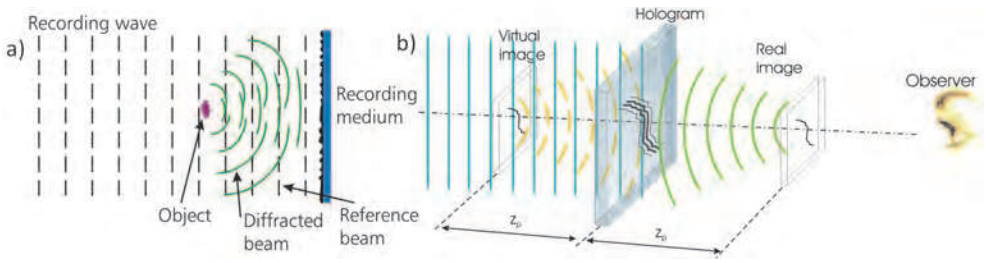

Fig. 1. Holographic recording scheme a) using Gabor's in-line configuration. The interference pattern between flat wavefront (reference beam) and beam diffracted from the object (object beam) is stored in the recording medium. Optical reconstruction b): the transmission hologram is illuminated by the reconstruction beam (the same as reference beam) and the image of the object appears where the object was initially located during the recording phase.

The first term is a background, the second is very small due to Gabor holography requirement for the object with high transmittance, thus the $|o(x,y)|^2 \to 0$. The wavefront diffracted from complicated transmission diffraction grating (hologram) converges behind the hologram generating the real image (fourth term $\sim o^*(x,y)$) while divergent wavefront generates the virtual image in front of the hologram where the object was placed during the recording step (third term $\sim o(x,y)$). The reconstructed intensity image is then $U(x,y) = u(x,y) \cdot u^*(x,y)$.

In recent experiments a high spatial resolution photoresist, usually utilized in electron beam lithography, was used for the recording of large numerical aperture (NA) holograms (Wachulak et al., 2006, 2007, 2008b). After developing, the holographic interference pattern was translated into a relief pattern in the surface of the photoresist and digitized using an atomic force microscope (AFM). Digitized hologram was used as an input for a numerical

code that reconstructs the image using a Fresnel propagator. This calculation back-propagates the object beam wavefront to obtain the amplitude and phase distribution of the field in the image plane (Goodman, 1996; Schnars & Juptner, 1994, 2002). To evaluate Fresnel-Kirchhoff integral, the product of spatial frequency representation of the hologram, obtained through a two dimensional fast Fourier transformation, and a quadratic phase free space Fresnel propagator in the spatial frequency domain was computed. Using this method the reconstruction of the hologram was performed numerically.

3.1 Coherence limitation to the spatial resolution in EUV holography

A photoresist was used to record the hologram. The interference pattern was converted into a height modulation after the developing process. To reconstruct the hologram a digitization is necessary. The digitization converts the photoresist height modulation into a gray-scale image that can be processed numerically in order to reconstruct the object.

The spatial resolution of the holographic recording is dictated by a numerical aperture $NA = n \cdot \sin(\Theta)$, where Θ is a maximum half-angle of cone of light that can enter the imaging system and n is an index of refraction of a medium. Also, the spatial resolution depends on the resolution of the recording medium. Consequently, the highest spatial frequency that can be recorded in the recording medium sets a limit to the NA. To avoid this limitation the holograms were recorded in a high resolution photoresist, PMMA, that has the spatial resolution of ~ 10nm for e-beam exposure (Hoole et al., 1997, Yamazaki et al., 2004).

The spatial resolution of the hologram is also limited by spatial and temporal coherence of illumination source and by digitization process. The coherence limitations to the hologram NA manifest themselves when a path difference between radiation diffracted by the object and reference beam exceeds either the longitudinal or transverse coherence lengths. The spatial resolution is often given by:

$$\Delta = \frac{a \cdot \lambda}{NA} \tag{7}$$

where $a \in <0.3,1>$ depending on the method used to measure the resolution and coherence of the source (Heck et al., 1998), λ is the wavelength of the illumination.

The limitation to the resolution set by the spatial coherence can be understood by the scheme depicted in Fig. 2. The reference beam and the beam diffracted from the point object will interfere only within coherence area depicted as a circle, with coherence radius R_c. Beyond that region one can assume that the interference will not occur. If the angle between two beams is Θ_{sc} then the recording numerical aperture is equal to:

$$NA_{sc} = \frac{R_c}{\sqrt{R_c^2 + z_p^2}} \tag{8}$$

where z_p defines a distance from the object to the recording medium. The spatial resolution is thus limited to:

$$\Delta_{sc} = \frac{a\lambda\sqrt{R_c^2 + z_p^2}}{R_c} \tag{9}$$

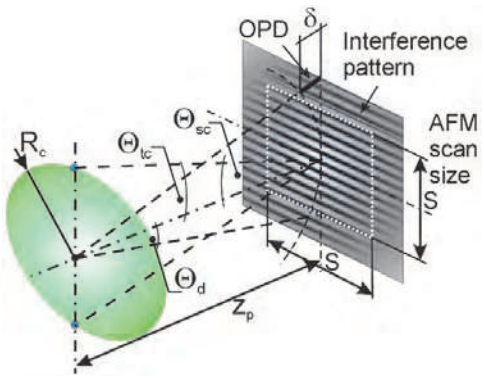

Fig. 2. Schematic description of spatial coherence, temporal coherence and scanning size limitations to the hologram spatial resolution.

The temporal coherence limits the recording numerical aperture as well. This can be seen in the scheme in Fig. 2 as well. The optical path difference δ between the reference and diffracted beams has to be smaller than coherence length of the illumination source $\delta \leq l_c$ in order to observe the interference. This limits region where the interference takes place, that can be defined by Θ_{tc} angle. The numerical aperture is thus restricted to:

$$NA_{tc} = \sqrt{1 - \left(\frac{z_p}{z_p + l_c} \right)^2} \tag{10}$$

and similarly the resolution:

$$\Delta_{tc} = \frac{a\lambda}{\sqrt{1 - \left(\frac{z_p}{z_p + l_c} \right)^2}} \tag{11}$$

Another limitation to the resolution is digitization process of the hologram. The resolution of reconstructed image is affected by scanning size s because for the object located at the center of scanning area, the finest interference fringes, carrying information about the highest spatial frequencies, are located at the edges of the scanned area. This can be related to the numerical aperture of the digitization as:

$$NA_d = \frac{s}{\sqrt{4z_p^2 + s^2}} \tag{12}$$

and similarly the spatial resolution:

$$\Delta_d = \frac{a\lambda\sqrt{4z_p^2 + s^2}}{s} \tag{13}$$

It is important to notice, that according to Equation (7) improvements to the resolution can be done either by decreasing the wavelength of illumination using an output of a short wavelength EUV source, or by increasing the numerical aperture in the recording and reconstruction steps. Decreasing distance between the object and recording medium allows for storing in the photoresist surface finer interference fringes, thus improving the resolution. During reconstruction, the AFM scan has to be large enough and with sufficiently fine sampling to read these fringes, to be able to reconstruct the information about corresponding spatial frequency components in the final, reconstructed image. The experiments, described in this chapter, will show, that increasing the recording and reconstruction NA allows to reach the resolution in EUV holographic imaging comparable to the wavelength of illumination.

3.2 Sampling considerations during the digitization process

The information about the highest spatial frequencies in the hologram has to be properly preserved in the recording medium and subsequently retrieved to reconstruct the image of the object with the highest possible resolution. For the simplest case of point objects corresponding Gabor holograms are Fresnel Zones (FZ). This simple hologram has a maximum spatial frequency defined by the outermost zone width Δr.

The resolution of the recording medium has to be better than the highest spatial frequency component in the hologram $\Delta_{rec} \leq \Delta r$, in order to faithfully reconstruct the object. Similarly pixel size in the AFM scans has to be equal or smaller than the highest spatial frequency component in the hologram $\Delta_{AFM} \leq \Delta r$. Given the relationship between the NA and Δr (Attwood, 1999), the minimum number of samples required for a given spatial resolution is:

$$N_{samples/line} = \frac{s}{\Delta r} \tag{14}$$

where s is the size of digitized hologram. The numerical aperture defined by the outermost zone width can be expressed as:

$$NA = \frac{\lambda}{2\Delta r} \tag{15}$$

Substituting Equation (7) yields to a resolution:

$$\Delta = 2a\Delta r \tag{16}$$

Moreover, using Equation (7) and digitization NA, expressed in terms of trigonometric functions $NA_d = \sin\left[\arctan\left(\frac{s}{2z_p}\right)\right]$, hologram scan size can be expressed as:

$$s = 2z_p \tan\left[\arcsin\left(\frac{a\lambda}{\Delta}\right)\right] \tag{17}$$

if $0 \leq \frac{a\lambda}{\Delta} \leq 1$. Finally the number of sample points obtained with the AFM in single scan line has to be equal to:

$$N_{samples/line} = \frac{2a \cdot s}{\Delta} = \frac{4az_p}{\Delta} \tan\left[\arcsin\left(\frac{a\lambda}{\Delta}\right)\right] \tag{18}$$

In case of small angle approximation it will be equal to:

$$N_{samples/line} = \frac{4a^2 z_p \lambda}{\Delta^2} \tag{19}$$

The total number of sampling points for two dimensional interference pattern can be expressed as:

$$N_{total} = \left(N_{sample/line}\right)^2 = \frac{16a^4 z_p^2 \lambda^2}{\Delta^4} \tag{20}$$

Equation (20) shows that the number of points in the digitalization, necessary to attain a given image spatial resolution Δ, scales as $N_{total} \sim \Delta^{-4}$. This imposes a practical limitation in Gabor's scheme if the distance z_p is not kept small. Due to the fact that the number of points per scan line in the AFM is often limited to 1024, 2048 etc., the NA is practically limited and the best option to increase the NA is to decrease the distance z_p.

4. Holographic 2-D imaging using EUV lasers

Two holograms of an atomic force microscope tip were obtained using a compact table top EUV laser in a Gabor's in-line configuration, as described in detail in (Wachulak et al., 2006). This configuration is very easy to set up and robust, moreover, it requires neither optics nor critical beam alignment.

4.1 Experimental details

In this experiment a table top discharge pumped capillary Ne-like Ar laser, radiating at 46.9 nm wavelength, was used for hologram recording. The laser was configured to produce 0.1 mJ pulses at repetition rate of 1 Hz. With a ratio $\lambda/\Delta\lambda \approx 10^4$, the capillary discharge laser has a longitudinal coherence length of $l_c \approx 470$ μm. Using Gabor's geometry, shown in Fig. 3, two holograms with two different NA were obtained by changing the distance between the object and the recording medium z_p. Two selected distances were $z_p \approx 4$ mm (NA = 0.038) and $z_p \approx 120$ μm (NA = 0.172). The temporal coherence limits the image spatial resolution to $\Delta \approx 64$ nm for $z_p = 4$ mm and $\Delta \approx 30$ nm for $z_p = 120$ μm. However, spatial coherence imposes a more severe limitation. In both cases this is the limiting factor to the maximum attainable resolution, $\Delta \approx 340$ nm for the smaller NA at $z_p \approx 4$ mm and $\Delta \approx 30$ nm in the second case.

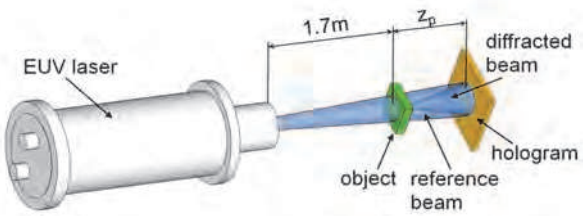

Fig. 3. Experimental set up used to record the EUV holograms in Gabor's configuration.

The recording was done in a 120 nm thick layer of PMMA (MicroChem 950,000 molecular weight) spin-coated on top of a silicon wafer. Exposures of approximately 100 seconds were necessary with the experimental set up utilized in this work. After the exposure, the photoresist was developed using a standard procedure: the sample was immersed in a solution of MIBK - methyl isobutyl ketone (4-Methyl-2-Pentanone) with IPA (isopropyl alcohol) 1:3 for 30 seconds and rinsed with IPA for 30 seconds. Finally the sample was dried using compressed nitrogen.

4.2 Results of 2-D holographic imaging with EUV laser

The exposure was adjusted to be in region of linear response of the photoresist and consequently a relief pattern height printed in its surface was equivalent to the interference intensity pattern of the hologram. The developed photoresist surface was mapped with the AFM to generate digitized holograms. Fig. 4a shows the hologram with low numerical aperture (NA = 0.038) recording, digitized area ~300x300 μm^2, and pixel size corresponding to 270 nm, while Fig. 4c depicts digitized hologram with higher numerical aperture (NA = 0.172). In this case the area scanned is 42x42 μm^2 with pixel size equivalent to 41 nm. The holograms were reconstructed by numerically simulating illumination with a short wavelength EUV readout wave. The amplitude and phase distributions of the field in the image plane were obtained calculating the field emerging from the hologram illuminated by a plane reference wave and numerically back-propagating the fields with a Fresnel propagator (Schnars & Juptner, 2002). The reconstructed image was found by taking two dimensional inverse fast Fourier transform (2D-IFFT) of the product of spatial frequency Fresnel propagator and the 2D-FFT of the hologram. This calculation allowed to obtain the amplitude and phase distribution of the field in the image plane. Fig. 4b and Fig. 4d are, respectively, the reconstructed images of corresponding holograms shown in Fig. 4a and Fig. 4c. The inset in Fig. 4b is a magnified region showing the end of the tip. In both reconstructed images a triangular profile of the AFM tip is clearly revealed. In case of Fig. 4d it was evident after the reconstruction that the tip was broken and partially contaminated, as can be observed in protrusion, marked by an arrow, in the upper part of the tip.

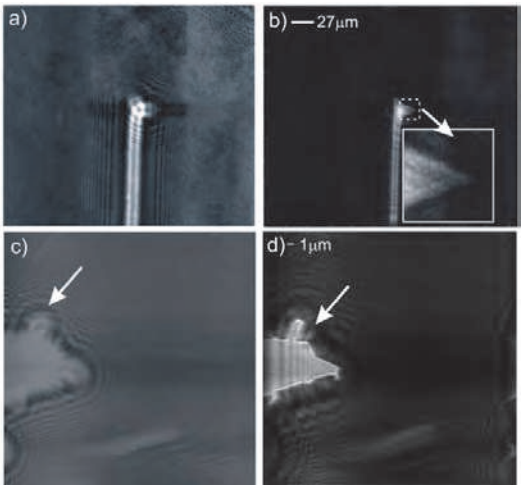

Fig. 4. Hologram recorded in surface of photoresist a) and reconstruction b) with low NA= 0.038 and, consequently, hologram c) and reconstruction d) with higher NA= 0.172.

4.3 Resolution estimation using wavelet decomposition and image correlation method

An optimum resolution in the reconstructed image was assessed by correlation with a synthesized image – template, used as a reference image. This reference image was constructed as a binary template that has by definition 1 pixel resolution. From the reference image a set of lower resolution images (wavelet components) was generated by wavelet decomposition of the reference image, each one having a spatial resolution relative to the reference image given by $Y = 2^X$, where Y is the relative resolution between the images in the wavelet decomposition and X is the order of the wavelet. In this case "haar" wavelet was applied. The reconstructed images were obtained by running the Fresnel propagator code with slightly different z_p around 4 mm and 120 μm, respectively. Then all reconstructions were correlated with the set of decreasing resolution wavelet components, shown in Fig. 5. To perform the correlation, higher wavelet orders were resized to have the same image size. The correlation coefficients between wavelet components and the reconstructed images for slightly different z_p provided a quantitative resolution of the reconstructions, relative to the synthesized reference images. This procedure also allowed for selection of an optimum reconstruction distance z_p. Fig. 5 shows a binary template that constitutes the order zero (X=0) wavelet component and the first four wavelet components with decreased resolution given by a factor 2^X.

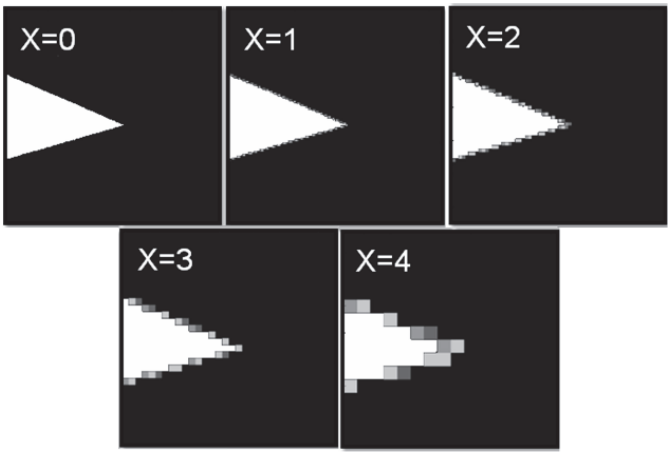

Fig. 5. Binary template (X=0) and wavelet components used to perform 2-D correlation with the reconstructed images to assess a relative resolution of the holograms.

Fig. 6 shows obtained correlation values for different images, reconstructed at different object-hologram distances z_p and different wavelet components, as a function of the wavelet scale X. By slightly changing the reconstruction distance the correlation coefficient changes but the shape of the curves remains unchanged.

Fig. 6a corresponds to smaller numerical aperture hologram (NA = 0.038). This plot shows that the largest value of the correlation function for all z_p corresponds to wavelet scale X = 0, and does not significantly change in the interval between X = 0 to X=1, decreasing faster for wavelet orders larger than 1. We conservatively assumed that the best correlation curve corresponds to X = 0.5, indicating that the resolution for this image is $2^{0.5} = 1.41$ relative to the reference image. The synthesized binary reference image has a pixel size of 270 nm and

consequently this analysis indicates that the reconstructed image has the spatial resolution equivalent to Δ=380 nm. Fig. 6b corresponds to higher numerical aperture recording (NA = 0.172). This plot clearly shows the maximum in the correlation values for X = 2 at all reconstruction distances ranging from 118 to 132 μm.

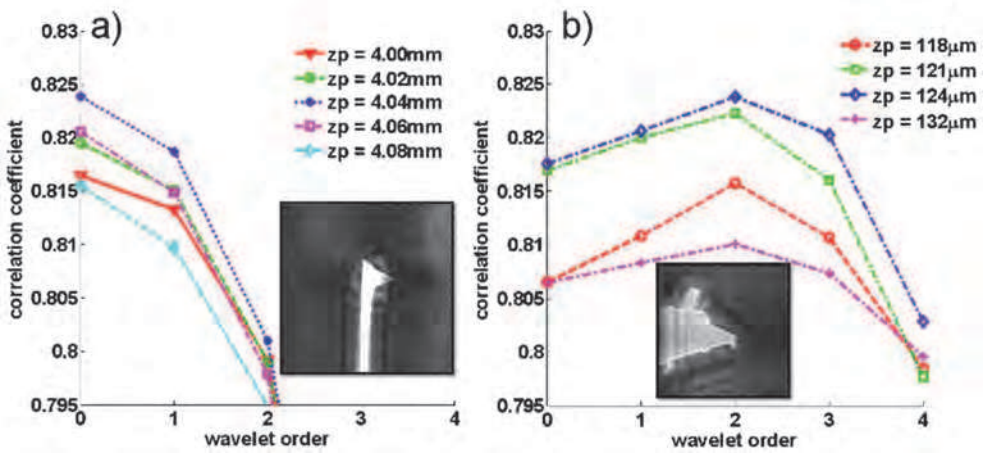

Fig. 6. Correlation values for different object-hologram distances z_p as a function of the wavelet scale X, a) recording with NA=0.038, pixel size 270 nm, b) recording with NA= 0.172, pixel size 41 nm.

This analysis indicates that the spatial resolution of the reconstruction is 4 pixels. In this case, the pixel size was 41 nm, setting the spatial resolution of the image to Δ=164 nm. Based on the recording NA, the spatial resolution limited by Rayleigh criterion Δ= (0.61 λ)/NA gives value of Δ_R=166 nm that compares very well with the results of wavelet analysis. The results are in good agreement with theoretical calculations and coherence limitations and were summarized in Table 1.

Rayleigh criterion based $a = 0.61$	Spatial coherence $\frac{a\lambda\sqrt{R_c^2 + z_p^2}}{R_c}$	Temporal coherence $\frac{a\lambda}{\sqrt{1-\left(\frac{z_p}{z_p + l_c}\right)^2}}$	AFM pixel size $\Delta_{AFM} = \Delta r$	AFM sampling limit $\Delta = 2a\Delta r$	Experimental resolution
z_p = 4 mm	337.8 nm	64.1 nm	270 nm	329.4 nm	380 nm
z_p = 120 μm	30.4 nm	29.2 nm	41 nm	50 nm	164 nm

Table 1. Coherence limitation to the resolution, AFM sampling limitations and experimentally obtained resolutions estimated based on the correlation analysis.

5. Wavelength resolution holography

5.1 Experimental setup

To reach near-ultimate spatial resolution z_p has to be reduced even further, according to Equations (7) and (20). A sample was composed of carbon nanotubes (CNT) with diameters between 50 and 80 nm and length 10-20 μm, placed on a 100 nm thick silicon membrane acting as a support. It was imaged using a table top EUV laser in Gabor's in-line configuration as depicted in Fig. 7 and described in more details in (Wachulak et al., 2008b).

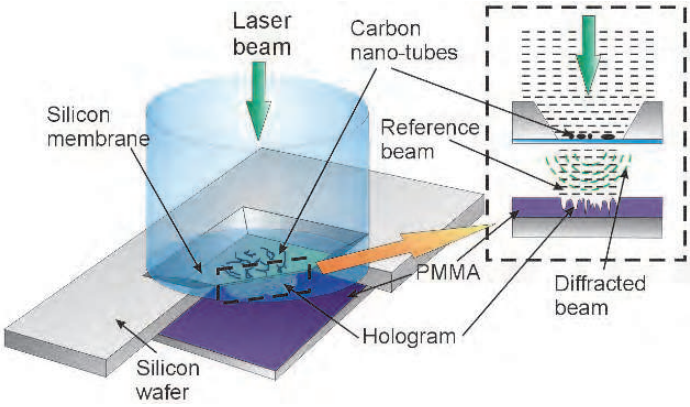

Fig. 7. Experimental setup in Gabor's hologram configuration. The EUV laser beam illuminates the object composed of carbon nano-tubes deposited on top of Si membrane.

The thin Si membrane has a transparency of approximately 60% at λ = 46.9 nm [1]. The sample was placed approximately z_p = 2.6 μm away from the Si wafer spin-coated with 120 nm thick layer of PMMA photoresist, resulting in recording NA practically equal to 1. However the limited area of the AFM scan that digitizes the hologram (9.9×9.9 μm^2) limits the NA to 0.88. The photoresist was later developed and the hologram stored in the resist was digitized with the AFM and numerically reconstructed using the same Fresnel propagator code. Fig. 8a,c show the holograms digitized with the AFM. The corresponding numerical reconstructions are shown in Fig. 8b,d. The CNTs are clearly visible as white lines in a black background.

The spatial resolution in the reconstructed image was found applying the knife-edge method. It is based on measuring 10-90% rise of the intensity in the line-cuts through the image. Two examples of such line-cuts depicted in Fig. 9a,b were taken in regions indicated in Fig. 8b,d. These cuts were realized in region where a "plateau" in the maximum and minimum intensities was clearly reached, to recreate the knife-edge resolution test. The measurements yielded the spatial resolution of ~46 nm. A mean value of resolution was found in similar cuts realized in different areas in the reconstructed images resulting in the statistical resolution of 45.8±1.9 nm, where error is assigned by a standard deviation spread in the measurements (Wachulak et al., 2008b).

[1] *from CXRO database, "http://www-cxro.lbl.gov/".*

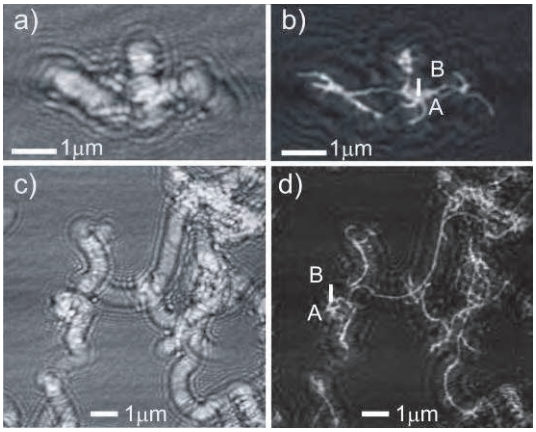

Fig. 8. a,c) Holograms and b,d) reconstructed images of 50-80 nm diameter carbon nanotubes. The holograms were obtained by scanning the photoresist surface with the AFM. Knife-edge test was applied to estimate the resolution of the reconstructed image in b,d).

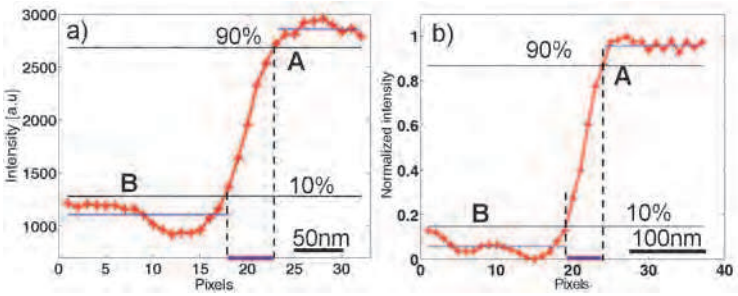

Fig. 9. The intensity lineouts through the reconstructions indicating a 10-90% intensity modulation over approximately 4.5 pixels. Figure a,b) corresponds to the reconstructed images in Fig. 8b,d) respectively. A mean value of multiple cuts obtained at different locations yielded the spatial resolution of 45.8±1.9 nm.

5.2 Gaussian filtering and correlation method for resolution and feature size assessment

To obtain a global assessment of the image spatial resolution, a correlation analysis on the reconstructed holograms was performed (Wachulak et al., 2008c). This method is based on the correlation between the reconstructed holographic image and a 2-D set of templates with calibrated resolution and diameter of the nanotubes, all generated from a master binary template. The set of master binary templates is derived from the original image, depicted in Fig. 10a, by skeletonizing the image, (Yatagai et al., 1982). The result of skeletonization is shown in Fig. 10b. It represents the shape of the nanotube, but has thickness of only 1 pixel. Then the skeleton is convolved with a set of circular templates of different diameters representing different diameters of the CNTs. One of those templates after the convolution is shown in Fig. 10c. From these master binary templates, a sub-set of templates with variable and calibrated resolutions was obtained by applying a Gaussian filter of variable

width. Fig. 10d shows one example of these templates, where the edges of the nanotube in Fig. 10c were blurred by the filtering process. Then the 2-D correlation between all the templates with variable resolution and variable nanotube diameter has been computed resulting in a 2-D correlation map. The global maximum in this map points out to the template that is the most similar to the reconstructed hologram. Both, resolution and nanotube diameter in the reconstructed image are the same as in the template that maximizes the correlation coefficient in the correlation map. Fig. 10e depicts the 2-D correlation map that indicates the CNT diameter equal to 70.6±5 nm and the spatial resolution 47.5±5 nm, where error is assigned as a one step in calculation of the surface shown in Fig. 10e.

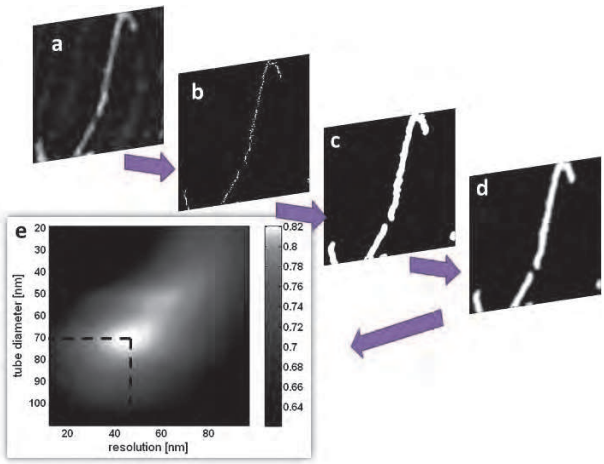

Fig. 10. Procedure to generate the templates with calibrated resolution. Filtered image a) with the low frequency background fluctuations removed. Skeletonizing b) of the image. Binary template c) obtained by convolution of the skeleton template (b) with a circular template. Template with degraded resolution d) obtained by convolution of the binary template (c) with a 2-D Gaussian filter. Correlation coefficients e) of the reconstructed image with different templates plotted as a function of nanotube diameter and template resolution. The nanotube diameter and resolution of the image are determined to be 70.6±5 nm and 47.5±5 nm by localizing a global maximum in the correlation plot.

The obtained resolution exceeds by ~19-21 nm the best possible obtainable resolution of 27 nm set by $\lambda/2\,NA$ (Jacobsen et al., 1990). Several factors degrade the resolution. It was verified that the spatial and temporal coherence of the laser source is not a limitation in this experiment, because $z_p << l_c$, R_c and NA~1. The longitudinal coherence length of the EUV laser is approximately l_c ~ 470 μm, $\Delta\lambda/\lambda \approx 10^{-4}$, and the spatial coherence radius is approximately 0.25 mm at the location of the recording, 0.75 m from the source (Liu et al., 2001). With these parameters, the spatial resolution set by the laser coherence properties is approximately 29 nm. Another limiting factor could arise from the digitalization because the AFM maps the hologram into a 1024×1024 matrix over a surface of approximately 9.9×9.9 μm², giving a pixel size of 9.7 nm. This pixel size sets the maximum spatial frequency that

can be recorded, establishing a limit for the spatial resolution of ~12 nm that practically does not play a role in this experiment. However, the resolution is affected by photoresist resolution (estimated to be ~20 nm for photon exposure (Solak et al., 1999)) and by resolution of the AFM that is defined by radius of curvature of the tip equal to 10 nm. The latter is not a fundamental limitation, as it can be overcome using a high resolution AFM tips. Taking all these factors in the convolution, the best possible resolution in our experiment is estimated to be ~39 nm, slightly better than the observed resolution. An additional possible factor degrading the resolution is roughness of Si membrane. Variations in the membrane's thickness can introduce a random background noise that degrades the image resolution. Detailed modeling indicates that a surface roughness of ~20 nm, which is similar to a measured roughness of the wafer that contains the membrane, would degrade the resolution to 45-46 nm adding a noise background similar to the noise measured in the reconstructed images.

6. Holographic 3-D imaging using EUV lasers

The possibility of volume three dimensional imaging by numerical sectioning obtained from a single high numerical aperture hologram (Wachulak et al., 2007) will be discussed in this section. Three dimensional images were obtained from Gabor holograms recorded in the photoresist after exposure using a table-top EUV laser. Digitized holograms were numerically reconstructed over the range of image planes by numerically sweeping the reconstruction distance, resulting in numerical optical sectioning of image depths.

6.1 Experimental details

The experimental set up is schematically illustrated in Fig. 11. The same source was used in this experiment as in the previous ones. The test object used in holographic volume imaging experiment consisted of a tilted metallic surface covered with opaque spherical markers.

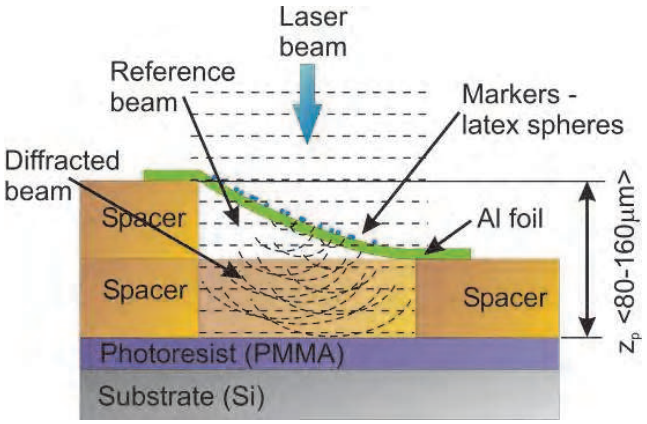

Fig. 11. Diagram of the 3-D EUV holography experimental set up showing details of the test object used.

This test object was fabricated by covering a semicircular hole 1.5 mm in diameter made in an 80 μm thick Mylar sheet with a 100 nm thick aluminum foil. The hole was partially covered

with a second Mylar sheet 80 μm thick, as schematically indicated in Fig. 11. The aluminum foil contours over the semicircular aperture to produce a variable height surface with desirable characteristics for this test and has a transmittance of approximately 35% at λ=46.9 nm limited mainly by a layer of native oxide [2]. The Al filter also suppresses lower photon energy plasma emission (i.e., long wavelength background) from the Ar laser source.
The object was prepared by placing a drop of water with heavily diluted latex spheres (2.62% solution in water) 465 nm in diameter, [3] on top of Al foil. Evaporation of the water left a random distribution of latex spheres (markers) deposited over the partially transparent tilted Al foil membrane. These spheres are completely opaque to 46.9 nm EUV laser radiation. With this deposition procedure, the markers are randomly distributed over the supporting Al foil and at predictable distances to the photoresist (heights) imposed by the foil profile. To activate the PMMA with 46.9 nm radiation requires exposures of 240 laser shots, 4 minutes exposure time at the repetition rate employed in this experiment. After exposure, the photoresist was developed using standard developing procedures.

6.2 Results of 3-D holographic imaging with EUV laser

Digitized hologram is shown in Fig. 12a. The digital reconstruction of the hologram digitized with the AFM is based on a numerical Fresnel propagator. Fig. 12a shows a small (42×42 μm²) section of the hologram. The numerical reconstruction of the hologram provided images of the object described above and shown in Fig. 12b.

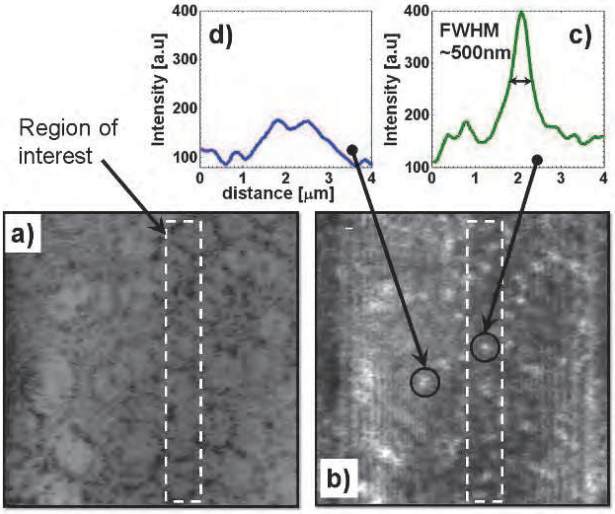

Fig. 12. Hologram of 3-D sample a) recorded in the photoresist surface and digitized with the AFM with a random distribution of 465nm diameter latex spheres - markers over tilted surface of Al foil. Numerical reconstruction b) of the hologram using Fresnel propagator algorithm. Intensity cuts in vertical direction of one marker that is "in focus" (c) and one "out of focus" (d). The white dotted lines indicate region in the reconstruction that is "in focus".

[2] *from CXRO database, "http://www-cxro.lbl.gov/".*
[3] *From Polysciences Inc.*

One of the critical parameters in the reconstruction code is a distance between the recording medium and the object, indicated in the diagram in Fig. 11 as z_p. Small changes in z_p reconstructs slightly different images. To determine the value of z_p corresponding to the optimum reconstruction, a 2-D image correlation was used and is described in details in references (Wachulak et al., 2006, 2007, 2008c).

To demonstrate retrieval of the depth information from the hologram the numerical reconstruction of the digitized hologram, shown in Fig. 12a, has to be performed for different values of distance z_p. The different runs produced different reconstructed images in which the latex spheres - markers located at the correct z_p generated a sharper image than those markers "out of focus". Fig. 12b shows one of these reconstructed images. In this case the reconstruction is optimum for z_p that matches height of a central part of the hologram, indicated in the figure by white dotted rectangle. In this region the height is such that the markers located there are reconstructed "in focus", while the latex spheres above and below this level are reconstructed blurred. This can be observed in Fig. 12c,d where the intensity profiles obtained in a vertical cut of one "in focus" marker (c) and one "out of focus" marker (d) are plotted. By changing z_p in the reconstruction code only the latex sphere markers located at the height equal to z_p produce sharper reconstruction images as compared to those markers out of focus. This is a similar effect to optical sectioning, however, performed on a digitally reconstructed image. The depth information in the hologram can finally be retrieved varying the reconstruction parameter z_p. To determine a value of z_p corresponding to the best reconstruction the reconstructed image was correlated with a template of the marker consisting of a circular mask with known size representing the latex sphere. Finding the maximum value of correlation between the reconstructed image of each marker and the mask determines corresponding optimum height. Combining this information with x-y coordinates of each marker allowed for placing each marker uniquely in a 3-D space and the reconstruction of surface of the test object with depth resolution.

Fig. 13a,c show the surface topography obtained from the reconstructed images in two different regions of the hologram. In case of Fig. 13a, the AFM scan was performed in region of the test object close to edge of Mylard spacer, where the slope of the Al foil is expected to be high. A similar scan performed at distance approximately 200 μm away from this edge, produced image with smaller slope, as shown in Fig. 13c. Fig. 13b,d show reconstructed heights for all markers as a function of transversal coordinate x in the same two regions of the object plotted in Fig. 13a,c. The surface plot from xyz space was projected into xz plane. These plots give a measure of spread of the calculated heights for all the markers and also show, as indicated by the best linear fit, different slopes in these two regions. The statistical dispersion of data points relative to the best linear fit are Δz = 2.64 μm for the region with high slope, Fig. 13b, and Δz = 1.32 μm for the region with lower slope Fig. 13d. This spread in the measured heights of markers compares well with expected accuracy in z direction determined by the NA of the hologram. As pointed out by Rogers, if one assumes the hologram as a superposition of Fresnel Zone Plates (FZPs) (Rogers, 1950), the resolution in z coordinate can be related to its depth of focus. For a FZP the depth of focus is given by $\delta z = \lambda / NA^2$ (Attwood, 1999). The NA corresponding to higher slope region, where z_p = 160 μm, is NA = 0.13, yielding a depth of focus δz = 2.77 μm. In region, where the Al foil has a lower slope, the latex markers were closer to the hologram, at a distance z_p = 140 μm. For this reconstruction the expected vertical resolution is δz = 2.12 μm.

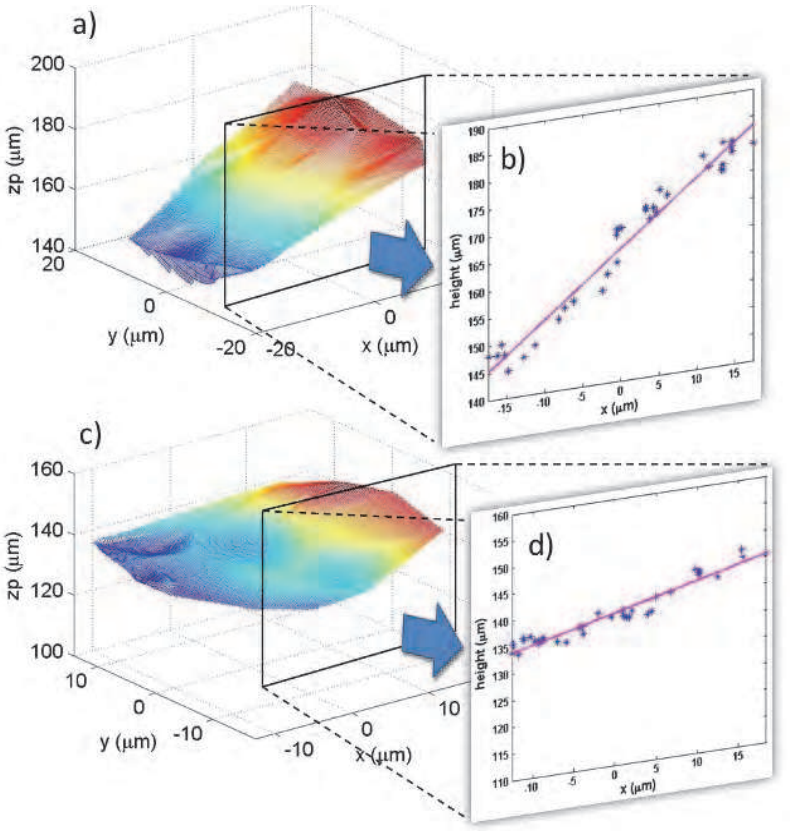

Fig. 13. Surface topographies obtained from reconstructed images and heights of the markers in different regions of the object. a), b) show the region close to the edge of the spacer where high slope is revealed in the Al foil while c), d) show region approximately 200 μm away from the edge with lower Al foil slope. b), d) are the projections of the 3-D plots on x-z plane to better visualize the slopes.

7. Conclusions

In this chapter the EUV table-top holographic imaging using a compact EUV laser as the illumination source was presented. The spatial resolution of the images of AFM tips, obtained by numerical reconstruction, was assessed utilizing a wavelet image decomposition and image correlation method leading to 164 nm. By increasing the numerical aperture of the recording and digitization wavelength-resolution EUV holograms were generated. The images were numerically reconstructed from the hologram recorded in surface of the photoresist and digitized with the AFM. Images of carbon nanotubes were obtained with 46±2 nm resolution determined by a knife edge test. Continuing development of highly coherent table-top EUV/SXR lasers in the vicinity of 10 nm (Wang et al., 2006) can be expected to enable future holographic imaging only limited by the photoresist resolution. Increasing flux of the EUV and SXR table top lasers opens a perspective in the future for

single shot recording, permitting full field time resolved holographic imaging. This imaging method allows hologram recording without any previous object preparation, as required in electron microscopy, and free of any interaction with a probe that may occur in scanning microscopes. Photon based imaging systems also allow spectroscopic contrast, an important characteristic in imaging with shorter wavelength radiation. It also opens the possibility to study specimens in different environments, for example in the presence of external magnetic or electric fields. Moreover detailed processing of the reconstructed holographic images, performed by changing object-hologram distance in the reconstruction code was presented. It enables retrieving the depth information from a single high NA hologram. Using a specially fabricated 3-D object the numerical reconstruction and analysis of the hologram allowed to map the surface topography with a depth resolution close to 2 μm.

8. Acknowledgements

This work was supported by the National Science Foundation ERC for Extreme Ultraviolet Science and Technology, Award Number EEC-0310717. The authors thank to Prof. Randy Bartels, Prof. Carmen Menoni and Prof. Jorge Rocca for their constructive comments and helpful discussions during the experiments presented herein.
First author would also like to acknowledge the support from Foundation for Polish Science, Homing 2009 Program, award number HOM/2009/14B, related to novel, high resolution imaging techniques.

9. References

Aoki, S.; Kikuta, S.; (1974). X ray holographic microscopy. *Jpn.J Appl.Phys.,* Vol. 13, pp. 1385

Attwood, D.T.; (1999). *Soft X-ray and extreme ultraviolet radiation*, Cambridge University Press, ISBN 0-521-65214-6, Cambridge, UK

Baez, A. V., (1952). A study in diffraction microscopy with special reference to X-rays. *Journal of the Optical Society of America*, Vol. 42, pp. 756

Bartels, R.A.; Paul, A.; Green, H.; Kapteyn, H.C.; Murnane, M.M.; Backus, S.; Christov, I.P.; Liu, Y.W.; Attwood, D.; Jacobsen, C.; (2002). Generation of spatially coherent light at extreme ultraviolet wavelengths. *Science*. Vol. 297, No. 5580, pp. 376-378

Chapman, H. N.; Hau-Riege, S.P.; Bogan, M.J.; Bajt, S.; Barty, A.; Boutet, S.; Marchesini, S.; Frank, M.; Woods, B.W.; Benner, W.H.; London, R.A.; Rohner, U.; Szoke, A.; Spiller, E.; Moller, T.; Bostedt, Ch.; Shapiro, D.A.; Kuhlmann, M.; Treusch, R.; Plonjes, E.; Burmeister, F.; Bergh, M.; Caleman, C.; Huldt, G.; Seibert, M. M.; Hajdu, J.; (2007). Femtosecond time-delay X-ray holography. *Nature*, Vol. 448, No. 9, pp. 676

Elsebitt, .S.; Schlotter, W. F.; Lorgen, M.; Hellwig, O.; Eberhardt, W.; Stohr, J.; (2004). Lensless imaging of magnetic nanostructures by X-ray spectro holography. *Nature*, Vol. 432, pp. 885-888

Gabor, D., (1948). A new microscopic principle. *Nature*, Vol. 161, pp. 777

Giles, J. W.; (1969). Image reconstruction from a Fraunhofer X-ray hologram with visible light. *Journal of the Optical Society of America*, Vol. 59, pp. 1179

Goodman, J. W.; (1996). *Introduction to Fourier Optics*. (3rd edition), Roberts & Company, ISBN 0-9747077-2-4, Englewood, Colorado, USA

Heck, J.M.; Attwood, D.T.; Meyer-Ilse, W.; Anderson, E.H.; (1998). Resolution determination in X-ray microscopy: an analysis of the effects of partial coherence and illumination spectrum. *Journal of X-Ray Science and Technology*. Vol. 8, pp. 95-104

Hoole, A. C. F.; Welland, M. E.; Broers, A. N.; (1997). Negative PMMA as a high-resolution resist - the limits and possibilities. *Semicond. Sci. Technol.* Vol. 12, pp. 1166-1170

Hun Lee, S.; Naulleau, P.; Goldberg, K. A.; Hyun Cho, C.; Tae Jeong, S.; Bokor, J.; (2001). Extreme-ultraviolet lensless Fourier-transform holography. *Applied Optics*, Vol. 40, No. 16, pp. 2655

Jacobsen, C.; Howells,M.; Kirz, J.; Rothman, S.; (1990), X-Ray Holographic Microscopy Using Photoresists, *Journal Of The Optical Society Of America A*, Vol.7, No.10, pp. 1847-1861

Leith, E. N.; Upatnieks J., (1962). Reconstructed Wavefronts And Communication Theory. *Journal of the Optical Society of America,* Vol. 52, pp. 1123

Lindaas, S.; Howells, H.; Jacobsen, C.; Kalinovsky, A.; (1996). X-ray holographic microscopy by means of photoresist recording and atomic-force microscope readout. *Journal of the Optical Society of America A*, Vol. 13, No. 9, pp. 1788-1800

Liu, Y.; Seminario, M.; Tomasel, F. G.; Chang, C.; Rocca, J. J.; Attwood, D. T.; (2001). Achievement of essentially full spatial coherence in a high-average-power soft-x-ray laser. *Physical Review A*, Vol. 63, No. 3, pp. 033802

Marchesini, S.; Boutet, S.; Sakdinawat, A. E.; Bogan, M. J.; Bajt, S.; Barty, A.; Chapman, H. N.; Frank, M.; Hau-Riege, S. P.; Szoke, A.; Cui, C.; Shapiro, D. A.; Howells, M. R.; Spence, J. C. H.; Shaevitz, J. W.; Lee, J. Y.; Hajdu, J.; Seibert, M. M.; (2008). Massively parallel X-ray holography. *Nature Photonics*, Vol. 2, pp. 560

McNulty,I.; Kirz, J.; Jacobsen, Ch.; Anderson, E. H.; Howells, M. R.; Kern, D. P.; (1992). High-Resolution Imaging by Fourier Transform X-ray Holography. *Science*, Vol. 256, No. 5059, pp. 1009-1012

Morlens, A.S.; Gautier, J.; Rey, G.; Zeitoun, P.; Caumes, J.P.; Kos-Rosset, M.; Merdji, H.; Kazamias, S.; Casson, K.; Fajardo, M.; (2006). Submicrometer digital in-line holographic microscopy at 32 nm with high-order harmonics. *Optics Letters*. Vol. 31, No. 21, pp. 3095-3097

Rogers, G.L.; (1950). Gabor diffraction microscopy. The hologram as a generalized zone-plate. *Nature*. Vol. 166, pp. 236-237

Rosenhahn, A.; Barth, R.; Staier, F.; Simpson, T.; Mittler, S.; Eisebitt, S.; Grunze, M.; (2008). Digital in-line soft x-ray holography with element contrast. *J. Opt. Soc. Am. A*, Vol. 25, No. 2, pp. 416

Rosenhahn, A.; Staier, F.; Nisius, T.; Schäfer, D.; Barth, R.; Christophis, Ch.; Stadler, L.M.; Streit-Nierobisch, S.; Gutt, Ch.; Mancuso, A.; Schropp, A.; Gulden, J.; Reime, B.; Feldhaus, J.; Weckert, E.; Pfau, B.; Günther, Ch. M.; Könnecke, R.; Eisebitt, S.; Martins, M.; Faatz, B.; Guerassimova, N.; Honkavaara, K.; Treusch, R.; Saldin, E.; Schreiber,S.; Schneidmiller, E.A.; Yurkov, M.V.; Vartanyants, I.; Grübel, G.; Grunze, M.; Wilhein, T.; (2009). Digital In-line holography with femtosecond VUV radiation provided by the free-electron laser FLASH. *Optics Express*, Vol. 17, No. 10, pp. 8220

Sandberg, R. L.; Paul, A.; Raymondson, D. A.; Hadrich, S.; Gaudiosi, D. M.; Holtsnider, J.; Tobey, R. I.; Cohen, O.; Murnane, M. M.; Kapteyn, H. C.; (2007). Lensless Diffractive Imaging Using Tabletop Coherent High-Harmonic Soft-X-Ray Beams. *Physical Review Letters*, Vol. 99, No. 098103, pp. 098103-1

Sandberg, R.L.; Song, C.; Wachulak, P.W.; Raymondson, D.A.; Paul, A.; Amirbekian, B.; Lee, E.; Sakdinawat, A.; Vorakiat, C.L.; Marconi, M.C.; Menoni, C.S.; Murnane, M.M.; Rocca, J.J.; Kapteyn, H.C.; Miao, J.; (2008). High numerical aperture tabletop soft x-ray diffraction microscopy with 70 nm resolution. *Proceedings of the National Academy of Science*, Vol. 105, No. 1, pp. 24-27

Sandberg, R.L.; Raymondson,D.; La-o-vorakiat,C.; Paul, A.; Raines, K.S.; Miao, J.; Murnane, M.M.; Kapteyn, H.C.; Schlotter, W. F.; (2009). Tabletop soft-X-ray Fourier transform holography with 50 nm resolution. *Optics Letters*. Vol. 34, No. 11, pp. 1618

Sayre, D.; Chapman, H.N.; Miao, J.; (1998). On the extendibility of X-ray crystallography to noncrystals. *Acta Crystallographica Section A*, Vol. 54, pp. 232-239

Schnars, U.; Juptner, W.P.O.; (1994). Digital recording and reconstruction of holograms in hologram interferometry and shearography. *Applied Optics*. Vol. 33, No. 20, pp. 4373-4377

Schnars, U.; Juptner, W.P.O.; (2002). Digital recording and numerical reconstruction of holograms. *Measurement Science & Technology*. Vol. 13, No. 9, pp. R85-R101

Solak, H. H.; He, D.; Li, W.; Singh, S.; Cerrina, F.; Sohn, B. H.; Yang, X. M.; Nealey, P., (1999). Exposure of 38 nm period grating patterns with extreme ultraviolet interferometric lithography, *Applied Physics Letters*, Vol. 75, No. 15, pp. 2328-2330

Thibault, P.; Dierolf, M.; Menzel, A.; Bunk, O.; David, Ch.; Pfeiffer, F.; (2008). High-Resolution Scanning X-ray Diffraction Microscopy. *Science*, Vol. 321, pp. 379

Tobey, R.I.; Siemens, M.E.; Cohen, O.; Murnane, M.M.; Kapteyn, H.C.; Nelson, K.A.; (2007). Ultrafast extreme ultraviolet holography: dynamic monitoring of surface deformation. *Optics Letters*. Vol. 32, No. 3, pp. 286-288

Trebes, J. E.; Brown, S. B.; Campbell, E. M.; Matthews, D. L.; Nilson, D. G.; Stone, G. F.; Whelan, D. A.; (1987). Demonstration of X-Ray holography with an X-Ray laser. *Science*, Vol. 238, No. 4826, pp. 517-519

Yamazaki, K.; Yamaguchi, T.; Namatsu, H.; (2004). Three-Dimensional Nanofabrication with 10-nm Resolution. *Jpn. J. Appl. Phys*. Vol. 43, pp. L1111-L1113

Yatagai, T.; Nakadate, S.; Idesawa, M.; Saito, H.; (1982). Automatic fringe analysis using digital image processing techniques. *Optical Engineering*. Vol. 21, pp. 901

Wachulak, P.; Bartels, R.A.; Marconi, M.C.; Menoni, C.S.; Rocca, J.J.; Lu, Y.; Parkinson, B.; (2006). Sub 400 nm spatial resolution extreme ultraviolet holography with a table top laser. *Optics Express*. Vol. 14, No. 21, pp. 9636-9642

Wachulak, P.; Marconi, M.C.; Bartels, R.A.; Menoni, C.S.; Rocca, J.J.; (2007). Volume extreme ultraviolet holographic imaging with numerical optical sectioning. *Optics Express*. Vol. 15, pp. 10622-10628

Wachulak, P. W.; Capeluto, M.G.; Menoni, C. S.; Rocca, J. J.; Marconi, M. C.; (2008). Nanopatterning in a compact setup using table top extreme ultraviolet lasers, *Opto-Electronics Review*, Vol. 16, No. 4, pp. 444–450

Wachulak, P.W.; Marconi, M.C.; Bartels, R. A.; Menoni, C. S.; Rocca, J.J.; (2008). Soft x-ray laser holography with wavelength resolution. *J. Opt. Soc. Am. B*. Vol. 25, No. 11, pp. 1811-1814

Wachulak, P.W.; Brewer, C.A.; Brizuela, F.; Chao, W.; Anderson, E.H.; Bartels, R.A.; Menoni, C.S.; Rocca, J.J.; Marconi, M.C.; (2008). Simultaneous determination of feature size and resolution in soft x-ray microscopy images. *Journal of the Optical Society of America B*. Vol. 25, pp. B20-B26

Wachulak, P. W.; Marconi, M. C.; Bartels, R. A.; Menoni, C. S.; Rocca, J. J.; (2010). Holographic imaging with a nanometer resolution using compact table-top EUV laser. *Opto-Electronics Review*, Vol. 18, No. 1, pp. 28-38

Wang, Y.; Granados, E.; Larotonda, M.A.; Berrill, M.; Luther, B.M.; Patel, D.; Menoni, C.S.; Rocca, J.J.; (2006). High-brightness injection-seeded soft-x-ray-laser amplifier using a solid target. *Physical Review Letters*. Vol. 97, No. 12, pp. 123901-123904

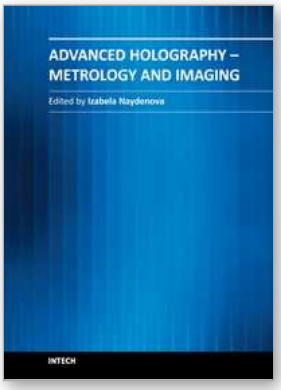

Advanced Holography - Metrology and Imaging

Edited by Dr Izabela Naydenova

ISBN 978-953-307-729-1
Hard cover, 374 pages
Publisher InTech
Published online 09, November, 2011
Published in print edition November, 2011

Advanced Holography - Metrology and Imaging covers digital holographic microscopy and interferometry, including interferometry in the infra red. Other topics include synthetic imaging, the use of reflective spatial light modulators for writing dynamic holograms and image display using holographic screens. Holography is discussed as a vehicle for artistic expression and the use of software for the acquisition of skills in optics and holography is also presented. Each chapter provides a comprehensive introduction to a specific topic, with a survey of developments to date.

InTech Europe
University Campus STeP Ri
Slavka Krautzeka 83/A
51000 Rijeka, Croatia
Phone: +385 (51) 770 447
Fax: +385 (51) 686 166
www.intechopen.com

InTech China
Unit 405, Office Block, Hotel Equatorial Shanghai
No.65, Yan An Road (West), Shanghai, 200040, China
中国上海市延安西路65号上海国际贵都大饭店办公楼405单元
Phone: +86-21-62489820
Fax: +86-21-62489821